Check for updates

ChemistryEurope
Excellence in Chemistry Research Worldwide

Research Article
doi.org/10.1002/ceur.202400020

www.journal.chemistry-europe.org

Activation of σ-Bonds by Group 13/Ylide-Based Ambiphiles: Understanding and Design

Daniel González-Pinardo,[a] Felix Krämer,[b] Frank Breher,*[b] and Israel Fernández*[a]

The factors controlling the activation of σ-bonds promoted by hidden Frustrated Lewis Pairs have been computationally explored using quantum chemical tools. To this end, the influence of both the nature of the group 13 element acting as Lewis acid as well as the cooperative action of the Lewis antagonists on the bond activation was quantitatively analyzed by means of the activation strain model of reactivity in combination with the energy decomposition analysis method. It is found that while the activation of the polar E^X–H bonds (E^{15} = group 15 element; E^{16} = group 16 element) is feasible, the analogous processes involving non-polar E^{14}–H bonds (CH_4, SiH_4 or H_2) proceed with much higher barriers. Nevertheless, these processes, and in particular the dihydrogen activation, can be realizable (i.e. proceeding with a feasible barrier) through rational design.

Introduction

While the activation of strong chemical bonds has traditionally been the domain of transition metal complexes,[1] the use of main-group species has emerged recently as a compelling alternative, mainly due to their significantly lower cost and reduced toxicity compared to transition metal complexes.[2] In this regard, Frustrated Lewis Pairs (FLPs), first introduced by D. Stephan in 2006,[3] should be specially highlighted as they are capable of not only achieving facile small molecule activation reactions (H_2, CO, CO_2, SO_2, etc.)[4] but also promoting other valuable transformations such as hydrogenations of unsaturated compounds (even in an enantioselective manner)[5] or polymerization reactions.[6]

Although the majority of FLPs are composed of group 13/15 combinations (typically, B/N, B/P and Al/P), other systems including heavier group 13 and group 14 elements,[7] or even transition metal fragments[8] in their structures, have been synthesized to enhance or even modify the reactivity of these species. In this context, we most recently described a system consisting of a phosphorus ylide featuring an aluminium Lewis acid in the *ortho* position of a phenyl ring scaffold (the so-called hidden FLP **1**, Scheme 1a).[9] This species not only splits the N–H bond of NH_3 in a reversible manner at ambient temperature but, strikingly, can be also used as a catalyst for ammonia transfer reactions to a variety of substrates, a challenging process even for transition metal chemistry.[10] In addition, we found that this and related species (including the gallium counterparts) can be also applied towards the activation of CO_2 and as catalysts for the reduction of CO_2 to methanol in the presence of pinacol borane (Scheme 1b).[11]

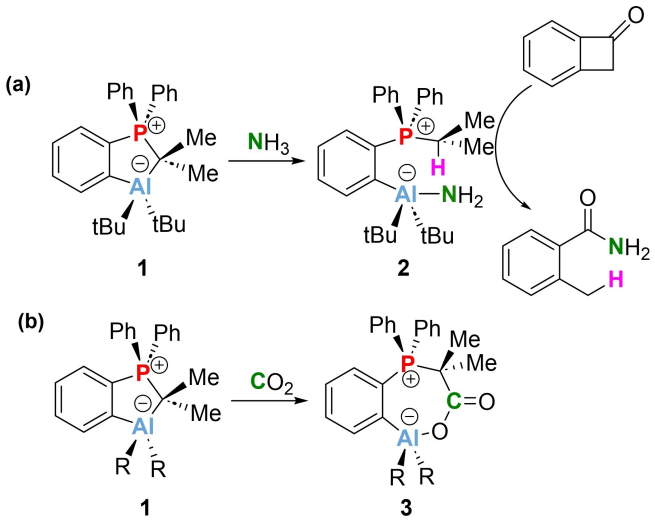

Scheme 1. Reactivity of hidden-FLP **1** towards the activation of NH_3 (a) and CO_2 (b). See references [9] and [11], respectively, for additional details.

Although the cooperative action of the Lewis antagonists has been proven to be responsible for the unique reactivity of classical FLPs,[12,13] very little is known about the mode of action of the acid/basic centers during the bond activation mediated by these hidden FLPs. In addition, the potential application of this and related group 13 species towards the activation of not only polar bonds (such as N–H or O–H) but also non-polar σ-bonds (particularly, dihydrogen activation) has not been explored so far. For this reason, we were prompted to carry out an

[a] D. González-Pinardo, Prof. Dr. I. Fernández
Departamento de Química Orgánica and Centro de Innovación en Química Avanzada (ORFEO-CINQA)
Facultad de Ciencias Químicas, Universidad Complutense de Madrid
28040 – Madrid (Spain)
E-mail: israel@quim.ucm.es

[b] Dr. F. Krämer, Prof. Dr. F. Breher
Institute of Inorganic Chemistry, Karlsruhe Institute of Technology (KIT)
Engesserstrasse 15, 76131 Karlsruhe (Germany)
E-mail: breher@kit.edu

Supporting information for this article is available on the WWW under https://doi.org/10.1002/ceur.202400020

© 2024 The Author(s). ChemistryEurope published by Chemistry Europe and Wiley-VCH GmbH. This is an open access article under the terms of the Creative Commons Attribution License, which permits use, distribution and reproduction in any medium, provided the original work is properly cited.

© 2024 The Author(s). ChemistryEurope published by Chemistry Europe and Wiley-VCH GmbH

Research Article
doi.org/10.1002/ceur.202400020

27514765, 2024, 3-4, Downloaded from https://chemistry-europe.onlinelibrary.wiley.com/doi/10.1002/ceur.202400020 by Spanish Cochrane National Provision (Ministerio de Sanidad), Wiley Online Library on [12/07/2024]. See the Terms and Conditions (https://onlinelibrary.wiley.com/terms-and-conditions) on Wiley Online Library for rules of use; OA articles are governed by the applicable Creative Commons License

extensive computational study to (i) understand the factors controlling the N–H activation reaction described by us recently,[9] (ii) explore the possible activation of other σ-bonds and (iii) design novel systems with enhanced reactivity. To this end, the trends in reactivity will be quantitatively analyzed in detail through the application of the Activation Strain Model (ASM) of reactivity[14] in combination with the Energy Decomposition Analysis (EDA) method.[15] This ASM-EDA approach was selected because it has greatly contributed to our current understanding of fundamental transformations in chemistry,[16] and particularly, of the mode of action and cooperativity of FLPs[13,17] and related main-group species.[18]

Results and Discussion

Activation of Ammonia and Related Group 15 Species

As previously reported,[9] hidden-FLP **1** is capable of splitting the N–H bond of NH_3 (1 atm) to produce species **2** in a reversible manner and at ambient temperature (Scheme 1a). According to our previous calculations, the process takes place stepwise where the formation of the Al–NH_3 bond with simultaneous rupture of the C_{ylide}–Al bond occurs first and is followed by the intramolecular migration of one proton of the Al–NH_3 moiety to the C_{ylide} atom. Similar results were found in the analogous profile involving the experimentally described[11] dimethyl-substituted system **1-Me** (Figure 1a), whose computed energies are also consistent with a reversible process ($\Delta G_R =$ 1.8 kcal/mol) occurring at room temperature ($\Delta G^{\neq} = 18.1$ kcal/mol).

To understand the cooperative action of the Lewis antagonists in this N–H bond activation reaction, we applied the Natural Orbital for Chemical Valence (NOCV)[19] extension of the Energy Decomposition Analysis (EDA) method. To this end, we selected key points along the reaction coordinate, namely, the initial reactant complex (having an Al···NH_3 distance of 2.386 Å), the first saddle point **TS1** (associated with the formation of the Al–N bond with concomitant Al–C_{ylide} bond-breaking), the resulting zwitterionic intermediate **INT1** and the final saddle point **TS2** (associated with the H-migration). Figure 1b shows snapshots of the corresponding NOCV deformation densities ($\Delta\rho$) together with their associated stabilization energies [$\Delta E(\rho)$]. As can be seen, at the beginning of the process, the principal charge depletion region (in red) corresponds to the lone-pair of the nitrogen atom whereas the charge accumulation (in blue) belongs to the partially vacant p_z-atomic orbital of the aluminum. This LP(N)→p_z(Al) orbital interaction (denoted as ρ_1) is the only significant orbital interaction between the reactants also in **TS1**. As the reaction progresses, it reinforces and becomes the main orbital contribution ($\Delta E(\rho_1) = -34.6$ kcal/mol) in **INT1**, where the formation of the Al–NH_3 bond is completely developed. Interestingly, in this intermediate the cooperative action of the ylide counterpart starts to take place as the donation from the C_{ylide} to the σ*(N–H) molecular orbitals becomes noticeable ($\Delta E(\rho_2) = -16.1$ kcal/mol). Not surprisingly, this LP(C)→σ*(N–H) orbital interaction continuously strengthens up to the transition state **TS2**, where it becomes ca. twice as strong as the LP(N)→p_z(Al) interaction (mainly as a result of the higher nucleophilicity of the ylide as compared to the NH_2 moiety). Therefore, our calculations indicate that the cooperative action of the Lewis antagonists of species **1** in the activation of NH_3 occurs in a highly asynchronous manner where the LP(N)→p_z(Al) orbital interaction takes place first and is responsible for both the polarization of the N–H bond and release of the lone-pair of the reactive ylide. The formation of the Al–N bond allows then the proton migration by the intramolecular nucleophilic attack of the C_{ylide} to the σ*(N–H) molecular orbital thus completing the stepwise bond activation. This asynchronous bond activation resembles that observed in classical FLPs,[13,17] which confirms the reactivity likeness of both species.

In addition, we also studied the activation reactions involving the heavier analogues of ammonia, i.e. PH_3 and AsH_3. From the data in Figure 1, it becomes clear that, although these reactions also proceed stepwise, they are kinetically much more difficult according to the computed high barriers ($\Delta G^{\neq} \approx 34$–40 kcal/mol). This can be, at least in part, ascribed to the lower donor ability of PH_3 or AsH_3 as compared to NH_3, which is confirmed by the lower value of $\Delta E(\rho 1)$ in **TS1**: −23.8 kcal/mol (NH_3) > −19.8 kcal/mol (PH_3) > −16.3 kcal/mol (AsH_3).

Activation of Water and Related Group 16 Species

Once the N–H bond activation was studied, we turned our attention to the analogous process involving the activation of the O–H σ-bond of water. Different from the reaction involving NH_3, our calculations indicate that the O–H activation occurs in a concerted manner where the transition state **TSw** is now associated with the simultaneous formation of the Al–O and C_{ylide}–H bonds with the concomitant rupture of the Al–C_{ylide} bond (Figure 2a). From the data in Figure 2a it becomes evident that the O–H activation, although also feasible at room temperature, is kinetically more difficult than the N–H activation ($\Delta\Delta G^{\neq} = 6.1$ kcal/mol), which can be initially ascribed to the higher O–H bond strength as compared to N–H (428 vs 314 kJ/mol, respectively).[20] At variance with the N–H activation, the O–H activation is clearly irreversible and strongly exergonic, which again can be ascribed to the much higher Al–O (512 vs 297 kJ/mol) bond strength.[20a]

Interestingly, the NOCV method indicates that in the transition state **TSw** the two main orbital interactions, namely LP(O)→p_z(Al) and LP(C)→σ*(O–H) (denoted as ρ_1 and ρ_2, respectively, Figure 2b), takes place simultaneously but, according to the computed stabilization energies, in a highly asynchronous manner ($\rho_1 > \rho_2$). Therefore, although this activation reaction is concerted, it also occurs in a highly asynchronous manner where the stronger LP(O)→p_z(Al) orbital interaction induces the polarization of the O–H bond and release of the lone-pair of the reactive ylide, therefore resembling the process involving the activation of ammonia.

We extended the O–H bond activation to the analogous group 13 element containing hidden-FLPs. From the data in

© 2024 The Author(s). ChemistryEurope published by Chemistry Europe and Wiley-VCH GmbH

Research Article
doi.org/10.1002/ceur.202400020

27514765, 2024, 3-4, Downloaded from https://chemistry-europe.onlinelibrary.wiley.com/doi/10.1002/ceur.202400020 by Spanish Cochrane National Provision (Ministerio de Sanidad), Wiley Online Library on [12/07/2024]. See the Terms and Conditions (https://onlinelibrary.wiley.com/terms-and-conditions) on Wiley Online Library for rules of use; OA articles are governed by the applicable Creative Commons License

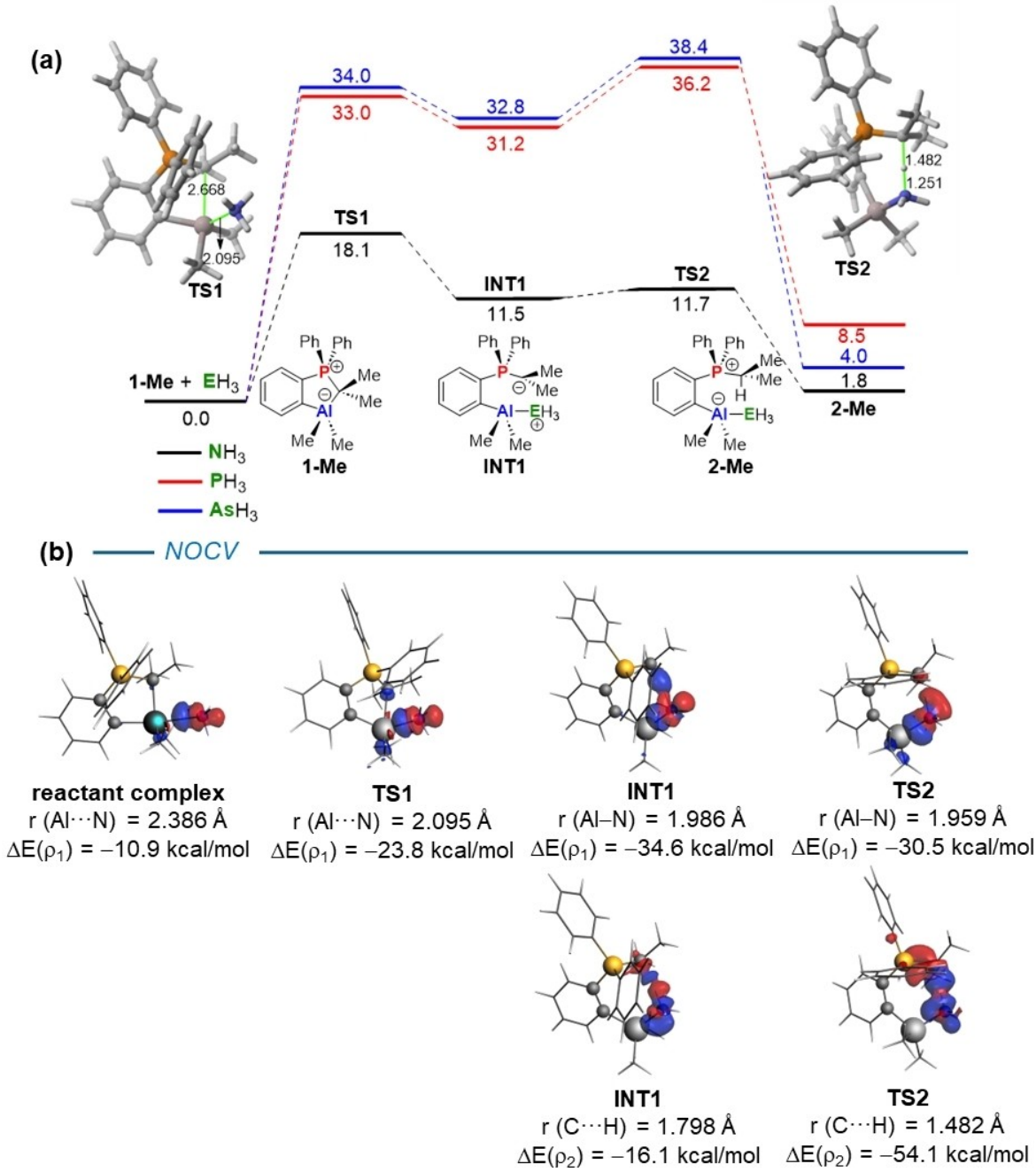

Figure 1. (a) Computed reaction profile for the $E^{15}H_3$-activation promoted by the aluminium hidden-FLP **1-Me**. Relative free energies (ΔG, at 298 K) and bond distances are given in kcal/mol and angstroms, respectively. All data have been computed at the PCM(benzene)-M06-2X/def2-TZVPP//PCM(benzene)-M06-2X/def2-SVP level. (b) Contour plots of the NOCV deformation densities ρ (isosurface value of 0.001 a.u.) and the associated energies ΔE(ρ) for the main orbital interactions occurring in the NH_3-activation mediated by **1-Me** along the reaction coordinate. The electronic charge flows from red to blue. All data were computed at the ZORA-M06-2X/TZ2P//PCM(benzene)-M06-2X/def2-SVP level.

Figure 2a, it becomes evident that the boron system is not reactive in view of the computed high barrier ($\Delta G^{\neq} = 38.0$ kcal/mol) which renders the OH activation mediated by **1-Me[B]** practically unfeasible. This is not surprising if we consider the much higher B–C bond strength as compared to its heavier group 13 counterparts (448 vs 255 kJ/mol, for B–C and Al–C bond, respectively)[20] which severely hampers the required ylide release in the transformation. Indeed, the computed E–C bond dissociation energy, calculated as the difference between the closed and open forms of **1-Me**, is higher for **1-Me[B]** ($\Delta G =$ 33.5 kcal/mol) as compared to **1-Me[Al]** ($\Delta G = 31.9$ kcal/mol), Scheme 2). At variance, the heavier analogues are clearly more reactive, in particular, the indium derivative **1-Me[In]**, which exhibits the lowest barrier for the O–H bond activation ($\Delta G^{\neq} =$ 17.4 kcal/mol) of the entire series.

Reasons for this reactivity trend, i.e. **1-Me[In]** > **1-Me[Al]** ≈ **1-Me[Ga]**, can be quantitatively analyzed with the help of the Activation Strain Model (ASM) of reactivity.[14] Figure 3 shows

© 2024 The Author(s). ChemistryEurope published by Chemistry Europe and Wiley-VCH GmbH

Research Article
doi.org/10.1002/ceur.202400020

27514765, 2024, 3-4, Downloaded from https://chemistry-europe.onlinelibrary.wiley.com/doi/10.1002/ceur.202400020 by Spanish Cochrane National Provision (Ministerio de Sanidad), Wiley Online Library on [12/07/2024]. See the Terms and Conditions (https://onlinelibrary.wiley.com/terms-and-conditions) on Wiley Online Library for rules of use; OA articles are governed by the applicable Creative Commons License

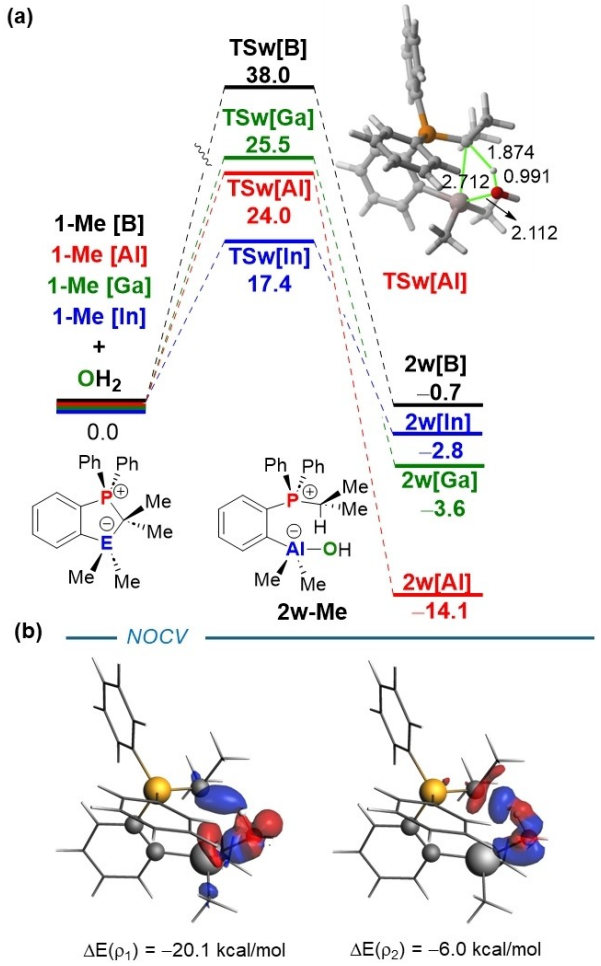

Figure 2. (a) Computed reaction profiles for the H_2O-activation promoted by the hidden-FLPs **1-Me**. Relative free energies (ΔG, at 298 K) and bond distances are given in kcal/mol and angstroms, respectively. All data have been computed at the PCM(benzene)-M06-2X/def2-TZVPP//PCM(benzene)-M06-2X/def2-SVP level. (b) Contour plots of the NOCV deformation densities ρ (isosurface value of 0.001 a.u.) and the associated energies ΔE(ρ) for the main orbital interactions occurring at transition state **TSw[Al]**. The electronic charge flows from red to blue. All data were computed at the ZORA-M06-2X/TZ2P//PCM(benzene)-M06-2X/def2-SVP level.

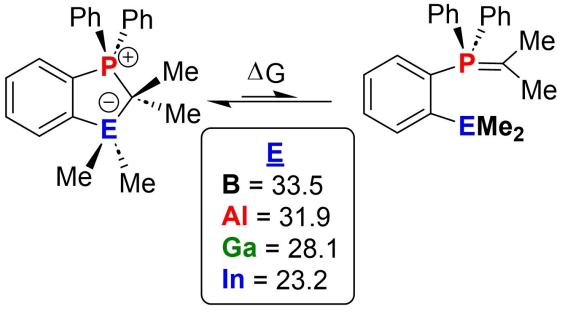

Scheme 2. Computed free energy differences between the closed and open forms of the hidden-FLPs **1-Me**. Energy values are given in kcal/mol and were computed at the PCM(benzene)-M06-2X/def2-TZVPP//PCM(benzene)-M06-2X/def2-SVP level.

the corresponding activation strain diagrams (ASDs) for the O–H activation reactions involving **1-Me** ([Al], [Ga] and [In])

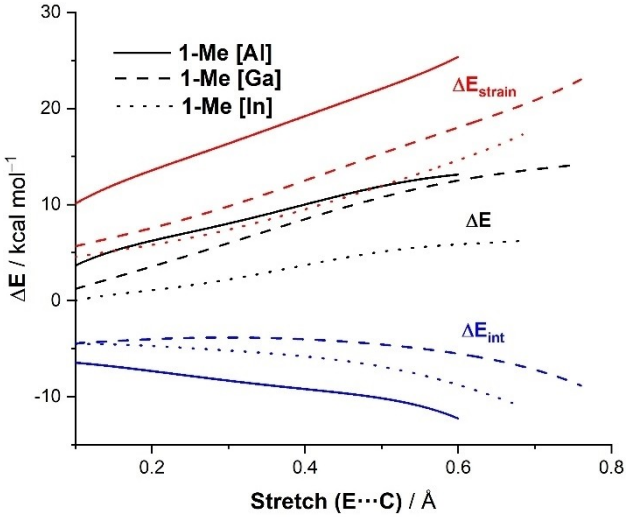

Figure 3. Comparative activation strain diagrams for the H_2O-activation reactions mediated by **1-Me[Al]** (solid lines), **1-Me[Ga]** (dashed lines) and **1-Me[In]** (dotted lines) along the reaction coordinate projected onto the stretch of the E–C bond. All data have been computed at the PCM(benzene)-M06-2X/def2-TZVPP//PCM(benzene)-M06-2X/def2-SVP level.

from the initial stages of the transformation upon the respective transition states and projected onto the stretch of the reactive $E–C_{ylide}$ bond. As graphically shown in Figure 3, the enhanced reactivity of the indium species is mainly due to the computed lower strain energy along the entire coordinate as compared to its lighter analogues. This occurs at the expense of the interaction energy between the deformed reactants, which is actually most stabilizing for the reaction involving **1-Me[Al]**. This finding therefore suggests that the **1-Me[In]** systems already possess an equilibrium geometry, which better fits that of the corresponding transition state, thus requiring comparatively less deformation than its lighter counterparts. This is directly related to the easiness of the ring opening, which can be again estimated as the difference between the closed and open forms of **1-Me** (ΔG = 23.2 kcal/mol for **1-Me[In]**, Scheme 2). Differently, the rather similar reactivity of the aluminum and gallium hidden FLPs is due to a combination of both strain and interaction terms. Thus, the **1-Me[Al]** system benefits from the strongest interaction between the reactants, but at the same time, it also exhibits the most destabilizing deformation energy. Although the interaction term is comparatively weaker in the process involving **1-Me[Ga]**, it benefits from a less destabilizing strain, and as a consequence, both systems, **1-Me[Al]** and **1-Me[Ga]**, exhibit rather similar activation barriers. Quite similar reactivity trends were found for the analogous process involving ammonia (see Supporting Information), which further supports the reactivity likeness of both activation reactions.

We also extended this study to the activation of the E^{16}–H bonds involving the heavier analogues of water, i.e. H_2S and H_2Se. Similarly, the activation of these E^{16}–H bonds also takes place in a concerted manner in one single reaction step. However, according to the computed energies, these analogous reactions proceed with higher activation barriers regardless of

© 2024 The Author(s). ChemistryEurope published by Chemistry Europe and Wiley-VCH GmbH

Research Article
doi.org/10.1002/ceur.202400020

27514765, 2024, 3-4, Downloaded from https://chemistry-europe.onlinelibrary.wiley.com/doi/10.1002/ceur.202400020 by Spanish Cochrane National Provision (Ministerio de Sanidad), Wiley Online Library on [12/07/2024]. See the Terms and Conditions (https://onlinelibrary.wiley.com/terms-and-conditions) on Wiley Online Library for rules of use; OA articles are governed by the applicable Creative Commons License

the nature of the group 13 element present in the hidden-FLP (see Table 1). Despite that, the same reactivity trend as that found for the activation of water, i.e. **1-Me[In]** > **1-Me[Al]** ≈ **1-Me[Ga]**, was found in the activation of its heavier H_2E^{16} counterparts, thus confirming the enhanced reactivity of the indium-FLP, which in addition leads to strongly exergonic reactions (ca. −20 kcal/mol).

The above results cannot be simply rationalized in terms of the relative E^{16}–H bond strengths, which actually follow the opposite trend as the activation barriers (428 vs 305 kJ/mol for O–H and Se–H bonds, respectively). Therefore, we decided to apply once again the ASM of reactivity for the processes mediated by the parent **1-Me[Al]** species as representative activation reactions. From the data in Table 1, which gathers the activation strain terms (i.e. computed at the corresponding transition states), it is clear that the lower barrier computed for the process involving H_2O as compared to the analogous reactions involving H_2S or H_2Se does exclusively derive from the strain term, which is less destabilizing for the **1-Me[Al]** + H_2O reaction. At variance, the interaction energy between the deformed reactants becomes rather similar for the three reactions. According to the EDA method, although the process involving H_2O benefits, not surprisingly, from a lower Pauli repulsion as compared to the analogous reactions involving H_2S or H_2Se, the latter processes exhibit comparatively stronger orbital interactions (coming mainly from the LP(X)→p_z(Al) orbital interaction, ρ_1). Both terms offset each other and, as a result, the total ΔE_{int} becomes rather similar.

Activation of Non-Polar σ-Bonds

Once the activation of polar bonds such as N–H or O–H bonds has been studied, we explored the ability of these hidden-FLPs to activate the more challenging non-polar σ-bonds. To this end, we selected the activation reactions mediated by the parent **1-Me[Al]** system involving H_2 and CH_4 along with its heavier group 14 analogs SiH_4 and GeH_4. Figure 4 shows the transition states associated with the activation of the corresponding E^{14}–H σ-bonds and gathers the computed respective activation and reaction energies. From the data in Figure 4, the activation of these non-polar, strong bonds occurs once again concertedly, in one single reaction step, where the E^{14}–H bond-breaking is associated with the simultaneous formation of the new Al–E^{14} and C_{ylide}–H bonds. The computed energies, and particularly the activation barriers, indicate that the activation

Table 1. Computed free activation ($\Delta G^{\neq}$)[a] and reaction (ΔG_R)[a] energies (in kcal/mol, computed at the PCM(benzene)-M06-2X/def2-TZVPP//PCM(benzene)-M06-2X/def2-SVP level) along with the ASM-EDA values (in kcal/mol, computed at the ZORA-M06-2X/TZ2P//PCM(benzene)-M06-2X/def2-SVP level) for the activation of H_2E^{16} (E^{16} = O, S, Se).

Energy	H_2O	H_2S	H_2Se
$\Delta G^{\neq}$[a]	24.0 (25.5) [17.4]	32.9 (29.7) [22.2]	29.8 (27.4) [21.1]
ΔG_R[a]	−14.1 (−3.6) [−2.6]	−8.5 (−8.2) [−13.9]	−11.3 (−11.9) [−18.7]
$\Delta E^{\neq}_{strain}$	25.0	33.1	32.0
$\Delta E^{\neq}$	12.9	22.5	19.7
$\Delta E^{\neq}_{int}$	−12.1	−10.5	−12.3
$\Delta E^{\neq}_{Pauli}$	79.1	102.4	100.4
$\Delta E^{\neq}_{elstat}$	−60.0	−54.3	−52.3
$\Delta E^{\neq}_{orb}$	−31.2	−58.6	−60.4
$\Delta E^{\neq}_{orb}(\rho 1)$	−20.1	−43.4	−46.9
$\Delta E^{\neq}_{orb}(\rho 2)$	−6.0	−8.4	−6.8

[a] Plain values refer to the processes mediated by **1-Me[Al]**, whereas values within parentheses and brackets refer to the activation reactions mediated by **1-Me[Ga]** and **1-Me[In]**, respectively.

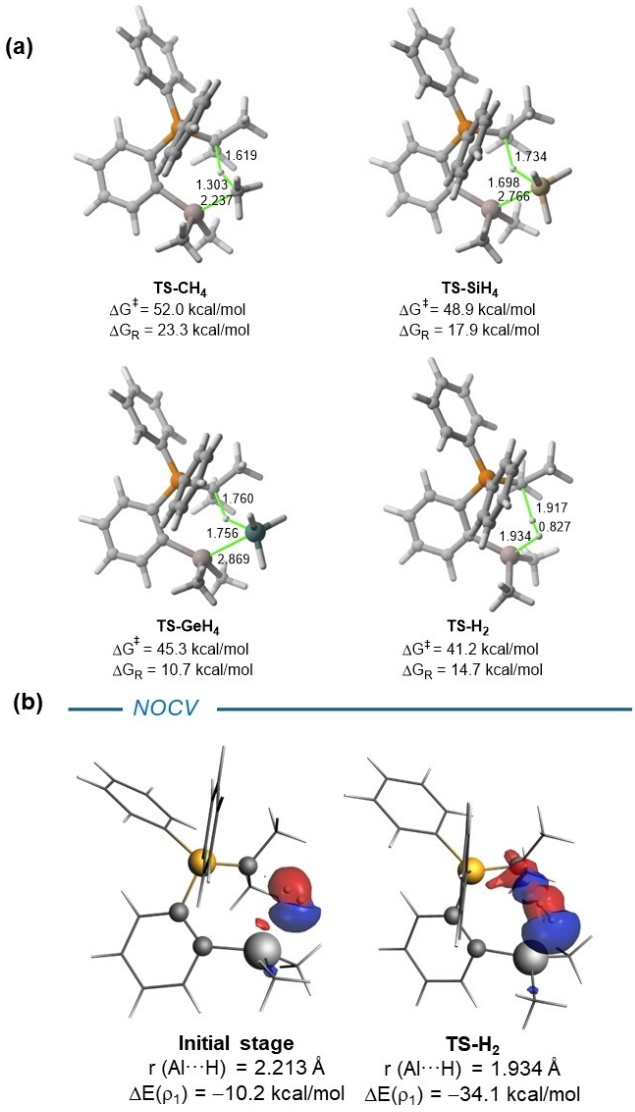

Figure 4. (a) Computed reaction profiles for the activation of nonpolar bonds promoted by the hidden-FLPs **1-Me[Al]**. Relative free energies (ΔG, at 298 K) and bond distances are given in kcal/mol and angstroms, respectively. All data have been computed at the PCM(benzene)-M06-2X/def2-TZVPP//PCM(benzene)-M06-2X/def2-SVP level. (b) Contour plots of the NOCV deformation densities ρ (isosurface value of 0.001 a.u.) and the associated energies ΔE(ρ) for the main orbital interactions occurring during the H_2-activation mediated by **1-Me[Al]**. The electronic charge flows from red to blue. All data were computed at the ZORA-M06-2X/TZ2P//PCM(benzene)-M06-2X/def2-SVP level.

© 2024 The Author(s). ChemistryEurope published by Chemistry Europe and Wiley-VCH GmbH

Research Article
doi.org/10.1002/ceur.202400020

27514765, 2024, 3-4, Downloaded from https://chemistry-europe.onlinelibrary.wiley.com/doi/10.1002/ceur.202400020 by Spanish Cochrane National Provision (Ministerio de Sanidad), Wiley Online Library on [12/07/2024]. See the Terms and Conditions (https://onlinelibrary.wiley.com/terms-and-conditions) on Wiley Online Library for rules of use; OA articles are governed by the applicable Creative Commons License

of these species is, not surprisingly, way more difficult than the activation of polar bonds. Indeed, in view of the computed barrier energies, the E^{14}–H (E^{14} = group 14 element) activation reactions mediated by **1-Me[Al]** are predicted to be unfeasible ($\Delta G \approx$ ca. 50 kcal/mol). At variance, the activation of the dihydrogen proceeds with a comparatively lower barrier of 41.2 kcal/mol. Although this value is still high, it opens the door for further optimization (see below). In any case, the non-polar E^{14}–H σ-bond activation reaction follows the same activation mode as the polar bonds in the sense that the transformation is initiated by the electron flow from the σ(E^{14}–H) molecular orbital to the p_z atomic orbital of aluminum (see Figure 4b for a snapshot of the main NOCV interaction at the beginning of the process). As the reaction progresses, this σ(E^{14}–H)→p_z(Al) orbital interaction continuously reinforces and polarizes the σ*(E^{14}–H) bond, which is then able to interact with the C_{ylide} at the proximities of the transition state region.

Given the importance of the activation of dihydrogen, as it constitutes the key step in different processes such as hydroformylation or hydrogenation of saturated compounds,[22] we then focused on the ways of reducing the relatively high barrier (ca. 40 kcal/mol) computed for the **1-Me[Al]** + H_2 reaction (see above). The first obvious modification should be, according to our previous result, the replacement of the aluminum center by the more reactive indium. Indeed, our calculations confirm that the analogous process mediated by **1-Me[In]** proceeds with a significantly lower barrier of 34.0 kcal/mol (Table 2), which can be now considered as a feasible reaction (occurring upon heating). Once again, it is found that the origin of this reduction of the barrier derives mainly from a markedly lower strain energy ($\Delta\Delta E^{\neq}_{strain}$ = 4.7 kcal/mol, Table 2), which results again from a more favorable ring-opening (see above).

Our previous NOCV analysis on the process indicates that the initial σ(H–H)→p_z(E) molecular orbital interaction is key for the process to occur. Therefore, we hypothesized that enhancing this interaction should result in a further lowering of the barrier. To this end, we first replaced the donor methyl groups directly attached to indium by more acceptor CF_3 groups. However, no beneficial effect was observed. Indeed, the barrier for the H_2-activation involving this system significantly increases mainly due to an increase in the strain energy (due to the high ring-openeing energy, ΔG = 33.1 kcal/mol) despite the σ(H–H)→p_z(In) interaction becomes stronger. We then modified the aryl tether connecting the Lewis antagonists and introduced strong electronegative groups (F or OMe) at the *ortho*- and *para*- positions relative to the indium atom. As shown in Table 2, although the effect is not dramatic, it is clearly confirmed that the presence of such groups in the aromatic ring further reduces the barrier to 31.7 kcal/mol (for the dimethoxy-substituted system), which is a ca. 10 kcal/mol difference with the respect to the parent process mediated by **1-Me[Al]**. Our ASM-EDA calculations also confirm that this further lowering of the barrier originates from a stronger interaction between the deformed reactants, which in turn derives from both stronger electrostatic and orbital interactions. The crucial role of the orbital interactions in the process and, particularly, the σ(H–H)→p_z(E^{13}) interaction (ρ_1) is further supported by the very good linear correlations found when plotting the barriers versus the computed ΔE_{orb} and $\Delta E_{orb}(\rho 1)$ values (correlations coefficients of R^2 = 0.97 and 0.98, respectively, see Figure 5). Therefore, it can be concluded that a process initially found unfeasible can efficiently take place through the proper modification of the initial hidden-FLPs guided by our ASM-EDA insights.

Conclusions

From the computational study reported herein, it can be concluded that whereas the activation of ammonia and its heavier group 15 counterparts PH_3 and AsH_3 promoted by the considered hidden-FLPs occurs stepwise in a reversible manner, the analogous processes involving group 16 elements (H_2O, H_2S, or H_2Se) are concerted, irreversible and proceed with slightly higher activation barriers. Despite that, all these transformations are similar in the sense that they are initiated by the LP(E→p_z(Al) orbital interaction which induces the polarization of the E^{16}–H bond and release of the lone-pair of the reactive

Table 2. Computed free activation ($\Delta G^{\neq}$)[a] energies (in kcal/mol, computed at the PCM(benzene)-M06-2X/def2-TZVPP//PCM(benzene)-M06-2X/def2-SVP level) along with the ASM-EDA values (in kcal/mol, computed at the ZORA-M06-2X/TZ2P//PCM(benzene)-M06-2X/def2-SVP level) for the activation of H_2.

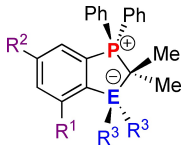

ER^3_2	R_1	R_2	$\Delta G^{\neq}$	$\Delta E^{\neq}$	$\Delta E^{\neq}_{strain}$	$\Delta E^{\neq}_{int}$	$\Delta E^{\neq}_{Pauli}$	$\Delta E^{\neq}_{elstat}$	$\Delta E^{\neq}_{orb}$	$\Delta E^{\neq}_{orb}(\rho_1)$
$AlMe_2$	H	H	41.2	32.1	35.4	−3.2	73.4	−35.5	−41.2	−34.1
$InMe_2$	H	H	34.0	26.1	30.7	−4.7	80.8	−39.3	−46.1	−41.5
$In(CF_3)_2$	H	H	42.1	33.3	36.4	−3.0	97.7	−47.4	−53.4	−44.2
$InMe_2$	F	H	33.5	24.8	30.6	−5.8	80.2	−38.6	−47.4	−43.5
$InMe_2$	F	F	33.4	24.9	30.7	−5.8	80.9	−38.8	−47.9	−44.0
$InMe_2$	OMe	H	32.2	23.3	30.9	−7.6	92.2	−42.7	−57.1	−52.6
$InMe_2$	OMe	OMe	31.7	23.3	31.0	−7.7	93.5	−43.2	−58.0	−53.5

© 2024 The Author(s). ChemistryEurope published by Chemistry Europe and Wiley-VCH GmbH

Research Article
doi.org/10.1002/ceur.202400020

27514765, 2024, 3-4, Downloaded from https://chemistry-europe.onlinelibrary.wiley.com/doi/10.1002/ceur.202400020 by Spanish Cochrane National Provision (Ministerio de Sanidad), Wiley Online Library on [12/07/2024]. See the Terms and Conditions (https://onlinelibrary.wiley.com/terms-and-conditions) on Wiley Online Library for rules of use; OA articles are governed by the applicable Creative Commons License

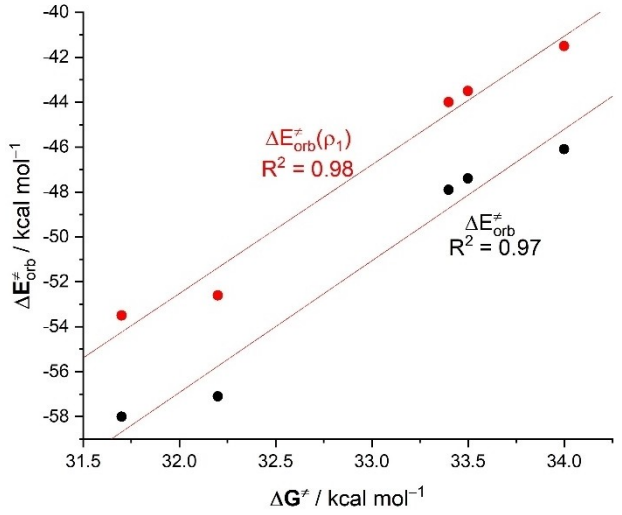

Figure 5. Plot of the computed activation barriers ($\Delta G^{\neq}$) versus the total orbital interactions ($\Delta E^{\neq}{}_{orb}$) and its main orbital component ($\Delta E^{\neq}{}_{orb}(\rho_1)$).

ylide. This indicates that even in concerted processes the cooperative action of the Lewis acid antagonists is not simultaneous but occurs in a highly asynchronous manner. Interestingly, the replacement of aluminum by gallium and, in particular, indium significantly enhances the reactivity of the hidden-FLP mainly because of a reduction in the required strain energy. Not surprisingly, the lack of reactive lone pairs in non-polar bonds (CH_4, SiH_4, GeH_4 or H_2) renders the activation of these species kinetically unfeasible. Nevertheless, through rational design, we have identified indium-based FLPs, where the aryl tether connecting both Lewis moieties is decorated with fluor and/or methoxy groups, as promising highly active systems capable of activating strong non-polar bonds.

Computational Details

Geometry optimizations of the molecules were performed without symmetry constraints using the Gaussian16 (RevB.01) suite of programs[21] at the dispersion-corrected M06-2X[22]/def2-SVP[23] level including solvent effects (solvent = benzene) with the Polarization Continuum Model (PCM) method.[24] Reactants and adducts were characterized by frequency calculations and have positive definite Hessian matrices. Transition states show only one negative eigenvalue in their diagonalized force constant matrices, and their associated eigenvectors were confirmed to correspond to the motion along the reaction coordinate under consideration using the Intrinsic Reaction Coordinate (IRC) method.[25] This level has been selected because it provides accurate energies[26] which are comparable to those obtained using the ωB97XD functional (see Table S1 in the Supporting Information). Energy refinements were carried out by means of single-point calculations at the same DFT level using the much larger triple-ζ basis set def2-TZVPP.[23] This level is denoted PCM(benzene)-M06-2X/def2-TZVPP//PCM(benzene)-M06-2X/def2-SVP. The computed thermochemistry data were corrected following Grimme's quasi-harmonic (QHA) model for entropy[27] using the GoodVibes[28] program at 298.15 K.

Activation Strain Model of Reactivity and Energy Decomposition Analysis

Within the ASM method,[14] also known as the distortion/interaction model,[14c] the potential energy surface $\triangle E(\zeta)$ is decomposed along the reaction coordinate, ζ, into two contributions, namely the strain $\triangle E_{strain}(\zeta)$ associated with the deformation (or distortion) required by the individual reactants during the process and the interaction $\triangle E_{int}(\zeta)$ between these increasingly deformed reactants:

$$\Delta E(\zeta) = \Delta E_{strain}(\zeta) + \Delta E_{int}(\zeta)$$

Within the EDA method,[15] the interaction energy can be further decomposed into the following chemically meaningful terms:

$$\Delta E_{int}(\zeta) = \Delta V_{elstat}(\zeta) + \Delta E_{Pauli}(\zeta) + \Delta E_{orb}(\zeta)$$

The term $\triangle V_{elstat}$ corresponds to the classical electrostatic interaction between the unperturbed charge distributions of the deformed reactants and is usually attractive. The Pauli repulsion $\triangle E_{Pauli}$ comprises the destabilizing interactions between occupied orbitals and is responsible for any steric repulsion. The orbital interaction $\triangle E_{orb}$ accounts for bond pair formation, charge transfer (interaction between occupied orbitals on one moiety with unoccupied orbitals on the other, including HOMO-LUMO interactions), and polarization (empty-occupied orbital mixing on one fragment due to the presence of another fragment). Moreover, the NOCV (Natural Orbital for Chemical Valence)[17] extension of the EDA method has been also used to further partition the $\triangle E_{orb}$ term. The EDA-NOCV approach provides pairwise energy contributions for each pair of interacting orbitals to the total bond energy.

The program package ADF[29] was used for EDA calculations using the optimized PCM(benzene)-M06-2X/def2-SVP geometries at the same M06-2X level in conjunction with a triple-ζ-quality basis set using uncontracted Slater-type orbitals (STOs) augmented by two sets of polarization functions with a frozen-core approximation for the core electrons.[30] Auxiliary sets of s, p, d, f, and g STOs were used to fit the molecular densities and to represent the Coulomb and exchange potentials accurately in each SCF cycle.[31] Scalar relativistic effects were incorporated by applying the zeroth-order regular approximation (ZORA).[32] This level of theory is denoted ZORA-M06-2X/TZ2P//PCM(benzene)-M06-2X/def2-SVP level.

Acknowledgements

We are grateful for financial support from grants PID2022-139318NB-I00 and RED2022-134331-T, funded by MICIU/AEI/10.13039/501100011033. The authors also acknowledge support by the German Research Foundation (DFG) through grant no BR 2169/5-1 (535548579).

Conflict of Interests

The authors declare no conflict of interest.

Data Availability Statement

The data that support the findings of this study are available in the supplementary material of this article.

© 2024 The Author(s). ChemistryEurope published by Chemistry Europe and Wiley-VCH GmbH

Research Article
doi.org/10.1002/ceur.202400020

Keywords: aluminum · hidden Frustrated Lewis Pairs · Phosphorus ylides · bond activation · DFT calculations

[1] See, for instance: a) J. F. Hartwig, in *Organotransition Metal Chemistry: From Bonding to Catalysis*, University Science Books, Mill Valley, CA, **2010**; b) M. Aresta, in *Carbon Dioxide as Chemical Feedstock*, Wiley-VCH, Weinheim, **2010**; c) B. M. Bhanage, M. Arai, in *Transformation and Utilization of Carbon Dioxide*, Springer-Verlag, Berlin, Heidelberg, **2014**; d) X. Lu, in *Carbon Dioxide and Organometallics*, Springer International Publishing, Switzerland, **2016**; e) *Nitrogen Fixation; Topics in Organometallic Chemistry*, 60, ed. Y. Nishibayashi, Springer, **2017**.

[2] a) P. P. Power, *Nature* **2010**, *463*, 171–177; b) T. Chu, G. I. Nikonov, *Chem. Rev.* **2018**, *118*, 3608–3680; c) Y. Su, R. Kinjo, *Chem. Soc. Rev.* **2019**, *48*, 3613–3659.

[3] G. C. Welch, R. R. San Juan, J. D. Masuda, D. W. Stephan, *Science* **2006**, *314*, 1124–1126.

[4] For leading reviews, see: a) D. W. Stephan, G. Erker, *Angew. Chem. Int. Ed.* **2010**, *49*, 46–76; *Angew. Chem.* **2010**, *122*, 50–81; b) G. Erker, *Pure Appl. Chem.* **2012**, *84*, 2203–2217; c) D. W. Stephan, G. Erker, *Top. Curr. Chem.* **2013**, *332*, *Frustrated Lewis Pairs I*; d) D. W. Stephan, G. Erker, *Chem. Sci.* **2014**, *5*, 2625–2641; e) D. W. Stephan, *J. Am. Chem. Soc.* **2015**, *137*, 10018–10032; f) D. W. Stephan, G. Erker, *Angew. Chem. Int. Ed.* **2015**, *54*, 6400–6441; *Angew. Chem.* **2015**, *127*, 6498–6541; g) D. W. Stephan, *Acc. Chem. Res.* **2015**, *48*, 306–316; h) D. W. Stephan, *Science* **2016**, *354*, aaf7229.

[5] a) J. Lam, K. M. Szkop, E. Mosaferi, D. W. Stephan, *Chem. Soc. Rev.* **2019**, *48*, 3592–3612; b) W. Meng, X. Feng, H. Du, *Acc. Chem. Res.* **2018**, *51*, 191–201; c) D. W. Stephan, *J. Am. Chem. Soc.* **2021**,*143*, 20002–20014.

[6] M. Hong, J. Chen, E. Y. Chen, *Chem. Rev.* **2018**, *118*, 10551–10616.

[7] Representative examples: a) W. Zheng, C. Pi, H. Wu, *Organometallics* **2012**, *31*, 4072–4075; b) B. Waerder, M. Pieper, L. A. Körte, T. A. Kinder, A. Mix, B. Neumann, H.-G. Stammler, N. W. Mitzel, *Angew. Chem. Int. Ed.* **2015**, *54*, 13416–13419; c) J. Possart, W. Uhl, *Organometallics* **2018**, *37*, 1314–1323; d) P. Holtkamp, F. Friedrich, E. Stratmann, A. Mix, B. Neumann, H.-G. Stammler, N. W. Mitzel, *Angew. Chem. Int. Ed.* **2019**, *58*, 5114–5118; e) L. Wickemeyer, N. Aders, A. Mix, B. Neumann, H.-G. Stammler, J. J. Cabrera-Trujillo, I. Fernández, N. W. Mitzel, *Chem. Sci.* **2022**, *13*, 8088–8094; f) L. Wickemeyer, I. Fernández, B. Neumann, H.-G. Stammler, N. W. Mitzel, *Angew. Chem. Int. Ed.* **2023**, *62*, e202216943.

[8] See, for instance: a) S. R. Flynn, D. F. Wass, *ACS Catal.* **2013**, *3*, 2574–2581; b) S. Arndt, M. Rudolph, A. S. K. Hashmi, *Gold Bull.* **2017**, *50*, 267–282; c) J. Campos, *J. Am. Chem. Soc.* **2017**, *139*, 2944–2947; d) N. Hidalgo, J. J. Moreno, M. Pérez-Jiménez, C. Maya, J. López-Serrano, J. Campos, *Chem. Eur. J.* **2020**, *26*, 5982–5993.

[9] F. Krämer, J. Paradies, I. Fernández, F. Breher, *Nat. Chem.* **2024**, *16*, 63–69.

[10] S. Streiff, F. Jérôme, *Chem. Soc. Rev.* **2021**, *50*, 1512–1521.

[11] F. Krämer, J. Paradies, I. Fernández, F. Breher, *Chem. Eur. J.* **2024**, *30*, e202303380.

[12] a) T. A. Rokob, A. Hamza, I. Papai, *J. Am. Chem. Soc.* **2009**, *131*, 10701–10710; b) T. A. Rokob, I. Bako, A. Stirling, A. Hamza, I. Papai, *J. Am. Chem. Soc.* **2013**, *135*, 4425–4437.

[13] a) D. Yepes, P. Jaque, I. Fernández, *Chem. Eur. J.* **2016**, *22*, 18801–18809; b) J. J. Cabrera-Trujillo, I. Fernández, *Chem. Commun.* **2019**, *55*, 675–678; c) J. J. Cabrera-Trujillo, I. Fernández, *Inorg. Chem.* **2019**, *58*, 7828–7836; d) J. J. Cabrera-Trujillo, I. Fernández, *Chem. Eur. J.* **2021**, *27*, 3823–3831.

[14] a) I. Fernández, F. M. Bickelhaupt, *Chem. Soc. Rev.* **2014**, *43*, 4953–4967; b) L. P. Wolters, F. M. Bickelhaupt, *WIREs Comput. Mol. Sci.* **2015**, *5*, 324–343; c) F. M. Bickelhaupt, K. N. Houk, *Angew. Chem. Int. Ed.* **2017**, *56*,10070–10086; *Angew. Chem.* **2017**, *129*, 10204–10221; See also: d) I. Fernández, in *Discovering the Future of Molecular Sciences* (Ed.: B.Pignataro), Wiley-VCH, Weinheim, **2014**, pp. 165–187.

[15] For reviews on the EDA method, see: a) F. M. Bickelhaupt, E. J. Baerends, in *Reviews in Computational Chemistry*, (Eds. K. B. Lipkowitz, D. B. Boyd), Wiley-VCH: New York, **2000**, Vol. 15, pp. 1–86; b) M. von Hopffgarten, G. Frenking, *WIREs Comput. Mol. Sci.* **2012**, *2*, 43–62; c) I. Fernández, in *Applied Theoretical Organic Chemistry*, (Ed. D. J. Tantillo), World Scientific, New Jersey, **2018**, pp. 191–226.

[16] Selected recent representative examples: a) D. N. Kamber, S. S. Nguyen, F. Liu, J. S. Briggs, H.-W. Shih, R. D. Row, Z. G. Long, K. N. Houk, Y. Liang, J. A. Prescher, *Chem. Sci.* **2019**, *10*, 9109–9114; b) A. Couce-Ríos, A. Lledós, I. Fernández, G. Ujaque, *ACS Catal.* **2019**, *9*, 848–858; c) I. Fernández, *Chem. Sci.* **2020**, *11*, 3769–3779; d) P. Vermeeren, T. A. Hamlin, I. Fernández, F. M. Bickelhaupt, *Angew. Chem. Int. Ed.* **2020**, *59*, 6201–6206; *Angew. Chem.* **2020**, *132*, 6260–6265; e) P. Vermeeren, T. A. Hamlin, I. Fernández, F. M. Bickelhaupt, *Chem. Sci.* **2020**, *11*, 8105–8112; f) T. A. Hamlin, F. M. Bickelhaupt, I. Fernández, *Acc. Chem. Res.* **2021**, *54*, 1972–1981; g) T. Hansen, P. Vermeeren, F. M. Bickelhaupt, T. A. Hamlin, *Angew. Chem. Int. Ed.* **2021**, *60*, 20840–20848; *Angew. Chem.* **2021**, *133*, 21008–21016.

[17] For a Feature article, see: I. Fernández, *Chem. Commun.* **2022**, *58*, 4931–4940.

[18] a) Y. García-Rodeja, F. M. Bickelhaupt, I. Fernández, *Chem. Eur. J.* **2016**, *22*, 13669–13676; b) B. Ghosh, J. J. Cabrera-Trujillo, I. Fernández, A. K. Phukan, *Inorg. Chem. Front.* **2022**, *9*, 5673–5687; c) S. Portela, I. Fernández, *Chem. Eur. J.* **2023**, *29*, e202300577; d) S. Ahmed, H. Das, D. González-Pinardo, I. Fernández, A. K. Phukan, *Chem. Eur. J.* **2024**, *30*, e202303746.

[19] M. P. Mitoraj, A. Michalak, T. Ziegler, *J. Chem. Theory Comput.* **2009**, *5*, 962–975.

[20] a) *Lange's handbook of chemistry*, 15th ed. J. A. Dean, chapter 4, McGraw-Hill, New York, **1999**; b) S. J. Blanksby, G. B. Ellison, *Acc. Chem. Res.* **2003**, *36*, 255–263.

[21] Gaussian16, Revision B.01, M. J. Frisch, G. W. Trucks, H. B. Schlegel, G. E. Scuseria, M. A. Robb, J. R. Cheeseman, G. Scalmani, V. Barone, G. A. Petersson, H. Nakatsuji, X. Li, M. Caricato, A. Marenich, J. Bloino, B. G. Janesko, R. Gomperts, B. Mennucci, H. P. Hratchian, J. V. Ortiz, A. F. Izmaylov, J. L. Sonnenberg, D. Williams-Young, F. Ding, F. Lipparini, F. Egidi, J. Goings, B. Peng, A. Petrone, T. Henderson, D. Ranasinghe, V. G. Zakrzewski, J. Gao, N. Rega, G. Zheng, W. Liang, M. Hada, M. Ehara, K. Toyota, R. Fukuda, J. Hasegawa, M. Ishida, T. Nakajima, Y. Honda, O. Kitao, H. Nakai, T. Vreven, K. Throssell, J. A. Montgomery, Jr., J. E. Peralta, F. Ogliaro, M. Bearpark, J. J. Heyd, E. Brothers, K. N. Kudin, V. N. Staroverov, T. Keith, R. Kobayashi, J. Normand, K. Raghavachari, A. Rendell, J. C. Burant, S. S. Iyengar, J. Tomasi, M. Cossi, J. M. Millam, M. Klene, C. Adamo, R. Cammi, J. W. Ochterski, R. L. Martin, K. Morokuma, O. Farkas, J. B. Foresman, D. J. Fox, Gaussian, Inc., Wallingford CT, 2016.

[22] Y. Zhao, D. G. Truhlar, *Theor. Chem. Acc.* **2008**, *120*, 215–241.

[23] F. Weigend, R. Ahlrichs, *Phys. Chem. Chem. Phys.* **2005**, *7*, 3297–3305.

[24] a) S. Miertuš, E. Scrocco, J. Tomasi, *Chem. Phys.* **1981**, *55*, 117–129; b) J. L. Pascual-Ahuir, E. Silla, I. Tuñón, *J. Comput. Chem.* **1994**, *15*, 1127–1138; c) V. Barone, M. Cossi, *J. Phys. Chem. A* **1998**, *102*, 1995–2001.

[25] C. Gonzalez, H. B. Schlegel, *J. Phys. Chem.* **1990**, *94*, 5523–5527.

[26] Y. Zhao, D. G. Truhlar, *Acc. Chem. Res.* **2008**, *41*, 157–167.

[27] S. Grimme, *Chem. Eur. J.* **2012**, *18*, 9955–9964.

[28] G. Luchini, J. V. Alegre-Requena, I. Funes-Ardoiz, R. S. Paton, *F1000Research* **2020**, *9*, 291.

[29] a) G. Te Velde, F. M. Bickelhaupt, E. J. Baerends, C. Fonseca Guerra, S. J. A. Van Gisbergen, J. G. Snijders, T. Ziegler, *J. Comput. Chem.* **2001**, *22*, 931–967; b) *ADF2020*, SCM, Theoretical Chemistry, Vrije Universiteit, Amsterdam, The Netherlands, http://www.scm.com.

[30] J. G. Snijders, P. Vernooijs, E. J. Baerends, *At. Data Nucl. Data Tables* **1981**, *26*, 483–574.

[31] J. Krijn, E. J. Baerends, *Fit Functions in the HFS-Method*, Internal Report (in Dutch), Vrije Universiteit Amsterdam, The Netherlands, 1984.

[32] a) E. van Lenthe, E. J. Baerends, J. G. Snijders, *J. Chem. Phys.* **1993**, *99*, 4597–4610; b) E. van Lenthe, E. J. Baerends, J. G. Snijders, *J. Chem. Phys.* **1994**, *101*, 9783–9792; c) E. van Lenthe, A. Ehlers, E. J. Baerends, *J. Chem. Phys.* **1999**, *110*, 8943–8953.

Version of record online: June 17, 2024

© 2024 The Author(s). ChemistryEurope published by Chemistry Europe and Wiley-VCH GmbH

27514765, 2024, 3-4, Downloaded from https://chemistry-europe.onlinelibrary.wiley.com/doi/10.1002/ceur.202400020 by Spanish Cochrane National Provision (Ministerio de Sanidad), Wiley Online Library on [12/07/2024]. See the Terms and Conditions (https://onlinelibrary.wiley.com/terms-and-conditions) on Wiley Online Library for rules of use; OA articles are governed by the applicable Creative Commons License